NeuroImage 202 (2019) 116144

Contents lists available at ScienceDirect

NeuroImage

journal homepage: www.elsevier.com/locate/neuroimage

Alterations in the functional brain network in a rat model of epileptogenesis: A longitudinal resting state fMRI study

Emma Christiaen [a,1,2,*], Marie-Gabrielle Goossens [b,1,2], Robrecht Raedt [b], Benedicte Descamps [a], Lars Emil Larsen [a,b], Erine Craey [b], Evelien Carrette [b], Kristl Vonck [b], Paul Boon [b], Christian Vanhove [a]

[a] MEDISIP, Department of Electronics and Information Systems, Ghent University, Corneel Heymanslaan 10, Ghent, Belgium
[b] 4Brain Team, Department of Head and Skin, Ghent University, Corneel Heymanslaan 10, Ghent, Belgium

ARTICLE INFO

Keywords:
Resting state functional MRI
Temporal lobe epilepsy
Intraperitoneal kainic acid rat model
Functional connectivity
Graph theory

ABSTRACT

Epilepsy is a neurological disorder characterized by recurrent epileptic seizures. Electrophysiological and neuroimaging studies in patients with epilepsy suggest that abnormal functional brain networks play a role in the development of epilepsy, i.e. epileptogenesis, resulting in the generation of spontaneous seizures and cognitive impairment. In this longitudinal study, we investigated changes in functional brain networks during epileptogenesis in the intraperitoneal kainic acid (IPKA) rat model of temporal lobe epilepsy (TLE) using resting state functional magnetic resonance imaging (rsfMRI) and graph theory. Additionally, we investigated whether these changes are related to the frequency of occurrence of spontaneous epileptic seizures in the chronic phase of epilepsy. Using a 7T MRI system, rsfMRI images were acquired under medetomidine anaesthesia before and 1, 3, 6, 10 and 16 weeks after status epilepticus (SE) induction in 20 IPKA animals and 7 healthy control animals. To obtain a functional network, correlation between fMRI time series of 38 regions of interest (ROIs) was calculated. Then, several graph theoretical network measures were calculated to describe and quantify the network changes. At least 17 weeks post-SE, IPKA animals were implanted with electrodes in the left and right dorsal hippocampus, EEG was measured for 7 consecutive days and spontaneous seizures were counted. Our results show that correlation coefficients of fMRI time series shift to lower values during epileptogenesis, indicating weaker whole brain network connections. Segregation and integration in the functional brain network also decrease, indicating a lower local interconnectivity and a lower overall communication efficiency. Secondly, this study demonstrates that the largest decrease in functional connectivity is observed for the retrosplenial cortex. Finally, post-SE changes in functional connectivity, segregation and integration are correlated with seizure frequency in the IPKA rat model.

1. Introduction

Blood oxygenation level dependent (BOLD) functional magnetic resonance imaging (fMRI) detects changes in blood oxygenation that are related to neuronal activity. It is a neuroimaging technique that allows visualisation of whole-brain activity and can be used to identify and investigate functional brain networks (Matthews and Jezzard, 2004). During rest, basic neuronal activity is believed to induce low frequency fluctuations in the BOLD signal that can be detected by performing resting state fMRI (rsfMRI). Calculating the correlation between the low frequency fluctuations, a technique called functional connectivity analysis, allows to identify brain regions that are functionally connected (Wang et al., 2010). The functional organization of the brain can be investigated using different analysis methods, including seed-based correlation, independent component analysis (ICA) and graph theory (Smitha et al., 2017). In graph theory, the brain is represented as a network consisting of nodes, usually brain regions, and edges that show

* Corresponding author.
E-mail addresses: emma.christiaen@ugent.be (E. Christiaen), mariegabrielle.goossens@ugent.be (M.-G. Goossens), robrecht.raedt@ugent.be (R. Raedt), benedicte.descamps@ugent.be (B. Descamps), larsemil.larsen@ugent.be (L.E. Larsen), erine.craey@ugent.be (E. Craey), evelien.carrette@uzgent.be (E. Carrette), kristl.vonck@ugent.be (K. Vonck), paul.boon@uzgent.be (P. Boon), christian.vanhove@ugent.be (C. Vanhove).
[1] These authors contributed equally to this work.
[2] Co-first authors.

https://doi.org/10.1016/j.neuroimage.2019.116144
Received 15 March 2019; Received in revised form 13 August 2019; Accepted 28 August 2019
Available online 29 August 2019

Abbreviations

Acb	nucleus accumbens
ALFF	amplitude of low frequency fluctuations
AP	anterior-posterior
Au	auditory cortex
BOLD	blood oxygenation level dependent
CA	cornu ammonis
Cg	cingulum
Cp	clustering coefficient
CPu	caudate putamen
DH	dentate hilus
DLO	dorsolateral orbital cortex
DRE	drug-resistant epilepsy
DV	dorsal-ventral
EEG	electroencephalography
Eg	global efficiency
Eloc	local efficiency
FOV	field of view
GE-EPI	gradient echo echo-planar imaging
GP	globus pallidus
Hip	hippocampus
Ins	insula
IPI	initial precipitating insult
IPKA	intraperitoneal kainic acid
KA	kainic acid
LMEM	linear mixed-effects model
Lp	characteristic path length
MC	motor cortex
ML	medial-lateral
NBS	network-based statistic
Pir	piriform cortex
PtA	parietal association cortex
PtP	posterior parietal cortex
ROI	region of interest
RSC	retrosplenial cortex
rsfMRI	resting state functional magnetic resonance imaging
SE	status epilepticus
Sep	septum
SSC	somatosensory cortex
TE	echo time
TeA	temporal association cortex
Th	thalamus
TLE	temporal lobe epilepsy
TR	repetition time
Vis	visual cortex

the relationship between the nodes. Several graph theoretical measures can be calculated to describe and quantify the network (Rubinov and Sporns, 2010). Changes in these measures, and thus in functional connectivity, have been found in various pathologies, including Alzheimer's disease, schizophrenia, attention-deficit hyperactivity disorder, traumatic brain injury and epilepsy (Wang et al., 2010).

Epilepsy is a neurological disorder characterized by recurrent epileptic seizures (Fisher et al., 2005). It is one of the most common brain disorders and in about one third of patients, seizures cannot be controlled with anti-epileptic drugs. These patients suffer from drug-resistant epilepsy (DRE) (Kwan and Brodie, 2000). In DRE, epilepsy is often caused by an initial precipitating insult (IPI) such as stroke, infection, trauma, brain tumor, or (febrile) status epilepticus (SE). An IPI is typically followed by a latent period, during which the brain is transformed into an epileptic brain, finally leading to chronic acquired epilepsy. This process is called epileptogenesis (Goldberg and Coulter, 2013).

In temporal lobe epilepsy (TLE), the most common type of acquired DRE (Engel Jr, 2014), structural abnormalities have been demonstrated in both patients and rodent models (Nairismagi et al., 2006; Niessen et al., 2005; Polli et al., 2014; Wolf et al., 2002). The volume of the hippocampus and the entorhinal, perirhinal and temporopolar cortices is lower in patients with TLE compared to healthy controls (Bernasconi et al., 2003; Briellmann et al., 2002; Jutila et al., 2001; Lencz et al., 1992; Marsh et al., 1997). In addition, significant differences in functional connectivity have been found (Liao et al., 2010; Morgan et al., 2015; Pittau et al., 2012; Song et al., 2015; Song et al., 2011a; Vlooswijk et al., 2011).

Studies combining rsfMRI with graph theory in patients with established epilepsy have shown abnormalities in the topological organization of the brain network. Most studies found a lower segregation in patients with TLE (Liao et al., 2010; Song et al., 2015; Vlooswijk et al., 2011), while integration was either increased (Liao et al., 2010; Song et al., 2015) or decreased (Vlooswijk et al., 2011). Functional connectivity was altered within the epileptic network, but also between the presumed epileptic network and the rest of the brain, including the contralateral equivalent of the epileptic network and the default-mode network (DMN) (Liao et al., 2010; Morgan et al., 2015; Pittau et al., 2012; Song et al., 2011a). Preclinical rsfMRI studies, in various rat models for acquired epilepsies, have demonstrated changes in functional brain networks compared to healthy rats (Bertoglio et al., 2019; Gill et al., 2017; Jiang et al., 2018; Mishra et al., 2014; Otte et al., 2012; Pirttimäki et al., 2016). In the intraperitoneal kainic acid (IPKA) rat model for TLE, Pirttimäki et al. (2016) found decreased functional connectivity, mainly between the somatosensory cortex and thalamus and between the perirhinal and piriform cortices, 1 or 2 months post-SE. Bertoglio et al. (2019) found a wide-spread network connectivity hyposynchrony 2 weeks post-SE and a severely affected functional connectivity in several regions of the DMN, including cingulate, parietal association and posterior parietal cortex. On the other hand, Gill et al. (2017) found a higher functional connectivity within the temporal regions, such as hippocampus and amygdala, and the limbic network and between the anterior and posterior DMN. However, there is still a need for longitudinal rsfMRI studies investigating network reorganisation during epileptogenesis, to provide more insight into the mechanisms of action of epilepsy.

In this study, graph theory analysis of rsfMRI-based functional brain networks was performed before and multiple times during SE-induced epileptogenesis and compared to healthy control rats. During the chronic epilepsy phase, at least 19 weeks post-SE, electroencephalography (EEG) monitoring was performed to quantify the frequency of occurrence of spontaneous seizures. The aim of this study was threefold: 1) to characterize how the functional organization of the rat brain changes after SE and during the development of TLE; 2) to identify brain regions with the highest degree of connectivity changes; 3) to evaluate whether connectivity changes are associated with the occurrence of spontaneous seizures. To the best of our knowledge, this is the first longitudinal rsfMRI study, combined with graph theory analysis, in a rat model of TLE.

2. Materials and methods

2.1. Animals

Twenty-seven adult male Sprague-Dawley rats (276 ± 15 g body weight; Envigo, The Netherlands) were used in this study. They were treated according to European guidelines (directive 2010/63/EU). The protocol was approved by the local Ethical Committee on Animal Experiments of Ghent University (ECD 16/31). For practical reasons, animals were divided over 3 batches ($n_{B1} = 10$, $n_{B2} = 5$, $n_{B3} = 12$) but

experiments were performed at a fixed age. Each batch included control animals. The animals were kept under environmentally controlled conditions (12 h normal light/dark cycles, 20–23 °C and 40–60% relative humidity) with food (Rats and Mice Maintenance, Carfil, Belgium) and water ad libitum. The animals were housed individually in type III H cages (Tecniplast, Australia) on wood-based bedding (Carfil, Belgium). Cages were enriched with paper nesting material (Nesting, Carfil, Belgium) and a gnawing wood (M-brick, Carfil, Belgium).

2.2. Status epilepticus

Twenty animals (8 weeks old) were intraperitoneally (i.p., 5 mg/kg/h) injected with kainic acid (KA; Tocris Bioscience, UK) according to the protocol of Hellier et al. (1998). KA was administered hourly until motor seizures were elicited for 3 h or longer, referred to as status epilepticus (SE). The other 7 animals were injected similarly with saline and used as control group. On average, the animals were injected with 12.2 mg/kg KA (range: 5–20 mg/kg). Two animals died during or within 4 h after SE induction.

2.3. Image acquisition

Anatomical and resting state functional MR images were acquired twice before the induction of SE and at 5 time points during the development of epilepsy: 1, 3, 6, 10 and 16 weeks after SE (Fig. 1). The two baseline scans, acquired 2–5 days apart, were used to assess the test-retest reliability of our methods and to obtain a better characterization of the baseline functional brain network. The animals were scanned in a random order, leading to an average difference in time of the day of 2 h and 53 min (range: 12 min–8 h and 6 min) between the baseline scans. Animals were transported to the MR facility one day before scanning. One IPKA rat was excluded 3 weeks after SE, because a metal fragment lodged behind its teeth caused a large artifact on the MR images.

During acquisition of the functional MR images the animals were sedated with medetomidine (Weber et al., 2006). First, the animals were anesthetized with isoflurane (5% for induction, 2% for maintenance; Isoflo, Zoetis, USA) and O_2. Then a bolus of medetomidine (0.05 mg/kg; Domitor, Orion Pharma, Finland) was injected subcutaneously and 10 min later, isoflurane anaesthesia was stopped. Fifteen minutes after the bolus injection, continuous subcutaneous infusion of medetomidine (0.1 mg/kg/h) was started and 25 min later functional MR images were acquired. After the image acquisition, anaesthesia was reversed with a subcutaneous injection of atipamezole (0.1 mg/kg; Antisedan, Orion Pharma, Finland).

The MR images were acquired on a 7T system (PharmaScan, Bruker, Germany) using a transmit volume coil (Rapid Biomedical, Germany) and an actively-decoupled rat head surface coil (Rapid Biomedical, Germany) to receive the signal. The body temperature of the animals was controlled using a circulating-water heating pad and respiration was measured using a pressure sensor. After optimizing the magnetic field homogeneity, TurboRARE T2-weighted anatomical images (TR 3661 m s, TE 37 m s, 30 slices, FOV $35 \times 35\ mm^2$, in-plane slice resolution $109 \times 109\ \mu m^2$, slice thickness 0.6 mm, acquisition time 9 min 46 s) were acquired. Then, 3 resting state fMRI scans per session were acquired using single-shot gradient echo echo-planar imaging (GE-EPI) with TR 2000 m s, TE 20 m s, 16 slices, FOV $30 \times 30\ mm^2$ and voxel size 0.375 x $0.375 \times 1\ mm^3$. Each scan comprised 300 repetitions and lasted 10 min. Examples of a GE-EPI scan of a representative IPKA animal at baseline and 16 weeks post-SE are shown in Figs. A1 and A2.

2.4. Electrode implantation

On average 19.5 weeks after SE (range 17–23 weeks), electrodes were implanted in both hippocampi for EEG recording. The rats were anesthetized with a mixture of isoflurane (5% for induction, 2% for maintenance) and medical O_2. After exposure of the skull, 13 small burr holes were drilled: 9 for positioning of stainless steel anchor screws (1.75 mm diameter; PlasticsOne, USA), 2 for the epidural ground/reference electrodes above right and left frontal cortex respectively, 1 for a left-sided hippocampal EEG recording electrode and 1 for a right-sided hippocampal EEG recording electrode. Epidural anchor screws were implanted to ensure sufficient fixation of the head cap during EEG monitoring in freely moving animals. Epidural electrodes were custom-made by attaching an insulated copper wire to an anchor screw. Bipolar recording electrodes were custom-made by twisting two polyimide-coated stainless steel wires (70 μm bare diameter; California Fine Wire, USA) around each other. The distance between wire tips was set at 900 μm.

Recording electrodes were inserted stereotactically in both hippocampi (AP -3.8 mm, ML±2.2 mm relative to bregma, DV about −3.3 mm relative to brain surface). Coordinates were selected based on Rat Brain Atlas by Paxinos and Watson (2013) and the T2-weighted anatomical MR images obtained 16 weeks after SE were used to ensure electrodes were placed outside KA-induced lesions. During electrode implantation, the position of the electrodes was verified by visual and auditive monitoring of real time electrophysiological recording, so that one tip of the electrode was positioned in the subgranular layer of the dentate gyrus, while the other tip was situated in the pyramidal cell layer of the CA1 region. All electrode leads ended in a connector that was fixed to the skull and anchor screws with acrylic dental cement. At the end of the surgery, rats were subcutaneously injected with the nonsteroidal anti-inflammatory drug meloxicam (1 mg/kg, Boehringer Ingelheim, Germany) and lidocaine (5% Xylocaine gel, AstraZeneca, UK) was locally applied to the wound to minimize discomfort. Twenty-four hours after surgery, rats received a second injection of meloxicam.

2.5. EEG recording

After a recovery period of one to two weeks, rats (IPKA group: n = 17, control group: n = 7) were connected to the EEG set up. The first 3 days of EEG recording served as an acclimatization period and were not used for further analysis. The EEG set up consisted of a custom-built head stage with unity gain preamplifier (based on TI TL074 JFET OpAmps), shielded 12-channel cables (363/2-000; PlasticsOne, USA), a 12-channel commutator (SL12C; PlasticsOne, USA) and a custom-built 512x amplifier (based on TI TL074 JFET OpAmps and a first order high-pass filter with a time constant of 1s). Recordings were performed while rats were awake and freely moving. Signals were sampled at 2 kHz by a 16-bit resolution data acquisition card (USB-6259, National Instruments, USA) and stored on the computer for offline analysis by a Matlab-based script (MathWorks, USA). Seizures were visually annotated by experienced investigators. An electrographic seizure was defined as a repetitive pattern (>2 Hz), of complex, high amplitude EEG spikes that lasts for a minimum of 5 s (Fig. A3). Average number of seizures/day and mean seizure duration were calculated based on 7 consecutive days of EEG recording.

Fig. 1. Timeline of the protocol. Anatomical and resting state fMRI were acquired 1 week before and 1, 3, 6, 10 and 16 after SE induction. On average 19.5 weeks after SE, electrodes were implanted in both hippocampi and 1 week later EEG was recorded in the animals for 7 consecutive days.

2.6. Data analysis

2.6.1. Preprocessing

The functional MRI data were preprocessed using SPM12 (https://www.fil.ion.ucl.ac.uk/spm/software/spm12/). First, images were corrected for differences in slice acquisition time; then, they were realigned to their mean image using a least squares approach and a 6 parameter (rigid body) spatial transformation to remove movement artifacts. Afterwards, the images were normalized to an EPI template and spatially smoothed using a Gaussian kernel with a Full Width at Half Maximum of 0.8 mm. Finally, a band pass filter (0.01 Hz–0.1 Hz) was applied to filter out low frequency and physiological noise.

2.6.2. Functional network construction

A parcellated atlas containing 38 cortical and subcortical regions of interest (ROIs) was manually constructed based on T2 anatomical images of the local population using SPM12 and Matlab. The ROIs are listed in Table 1. The atlas was adapted to the IPKA model. Structural damage visible on the T2 images as hyperintensity was excluded from the ROIs. Due to the resolution of the fMRI images, it was not useful to divide the hippocampus into its subregions. It was not possible to make an ROI of the entorhinal cortex, a brain region that is structurally damaged during epileptogenesis, because of EPI signal dropout as a result of air in the ear canal.

A Graph Theoretical Analysis Toolbox (GRETNA; Wang et al., 2015) was used to extract the mean time series of each ROI and to calculate the Pearson correlation coefficient between each pair. In this way a 38 x 38 correlation matrix was obtained. Thresholds were applied to this matrix to remove the weakest connections. These thresholds were chosen based on network density (i.e. the number of remaining connections divided by the maximum number of possible connections). Different thresholds were used to obtain correlation matrices with a density ranging from 20% to 50%. For further analysis, the correlation coefficients were Fisher r-to-z transformed to obtain a normal distribution. Based on the correlation matrices, functional networks or graphs were constructed, in which each node represents a ROI and each edge a correlation coefficient. In Fig. 2 an overview of the methodology for network construction is given.

2.6.3. Graph theoretical analysis

For each graph several network measures were calculated using GRETNA: degree was investigated on a nodal level, and characteristic path length (Lp), clustering coefficient (Cp), global efficiency (Eg) and local efficiency (Eloc) on a global level. Degree or connection strength is the number of edges connected to a node. It is a measure for centrality or the importance of a node in the network. Characteristic path length is the average number of edges connecting two nodes in the network and global efficiency is the average inverse path length between two nodes. Both are measures of functional integration or overall communication efficiency in the network. Clustering coefficient is the fraction of neighbours of a node that are also connected to one another and local efficiency is global efficiency calculated within the neighbourhood of a node, i.e. the nodes connected to that node. Both are measures of functional segregation or local interconnectivity (Rubinov and Sporns, 2010; Wang et al., 2010).

Network measures were calculated at each matrix density, from 20% to 50% density with a 1% interval, and averaged over these densities. Then the measures were averaged over the 3 scans acquired within one scanning session to obtain one value per animal per time point.

The test-retest reliability of the network measures was assessed by calculating the coefficient of variation between scans in the same scanning session, between different sessions and between different animals (Table A1).

Table 1
List of ROIs. Each ROI has a component on the left and right side of the brain.

ROIs			
Full name	Abbreviation	Full name	Abbreviation
Auditory Cortex	Au	Piriform Cortex	Pir
Caudate Putamen	CPu	Posterior Parietal Cortex	PtP
Cingulate Cortex	Cg	Prelimbic Cortex	PrL
Dorsolateral Orbital Cortex	DLO	Retrosplenial Cortex	RSC
Globus Pallidus	GP	Septum	Sep
Hippocampus	Hip	Somatosensory Cortex	SSC
Insula	Ins	Temporal Association Cortex	TeA
Motor Cortex	MC	Thalamus	Th
Nucleus Accumbens	Acb	Visual Cortex	Vis
Parietal Association Cortex	PtA		

2.6.4. Amplitude of low frequency fluctuations

The analysis of resting state fMRI using graph theory is based on the correlations of low frequency fluctuations in the BOLD signal. The amplitude of these fluctuations could have an influence on functional connectivity and should be taken into account when analysing resting state networks (Di et al., 2013). Therefore, mean amplitude of low frequency fluctuations (ALFF) in the frequency range 0.01–0.1 Hz was calculated in all ROIs using the Resting-State fMRI Data Analysis Toolkit (REST; Song et al., 2011b) and used as a covariate in the statistical analysis of the network measures.

2.6.5. Volumetric analysis of hippocampus

The hippocampus is one of the brain structures that is affected most by cell damage in the IPKA rat model (Lévesque and Avoli, 2013) and hippocampal volume loss is a known feature of IPKA animals (Polli et al., 2014; Wolf et al., 2002). We investigated volume loss in the hippocampus during epileptogenesis. The volume of the hippocampus was measured on the T2-weighted MR images using the image processing package Fiji, a distribution of ImageJ (Rueden et al., 2017; Schindelin et al., 2012). The hippocampus was drawn manually and its volume was calculated (Fig. 3A). Hyper- and hypointensities were considered damage and excluded from the volume. In other words, we calculated the volume of the hippocampus that appeared undamaged on the T2-weighted MR images, or the T2-normal hippocampal volume (Wolf et al., 2002). To avoid false correlations due to this structural damage, visible damage was excluded from all ROIs used to construct the functional brain network. The ROIs were adapted based on the T2 image of the animal with the most extensive structural damage (KAC4, 16 weeks post-SE), as can be seen in Fig. 3B. These ROIs were used in all animals, at all time points. We chose to use fixed ROIs because the size of an ROI can have an influence on its connectivity and larger ROIs tend to be more highly correlated (Fornito et al., 2010). If variable ROIs are used, a decreased hippocampal volume could falsely induce a lower correlation. The effect of using a reduced hippocampal ROI on the control animals' outcome values is minimal, as similar results were obtained using a hippocampal ROI that encompasses the whole hippocampus (data not shown).

2.6.6. Statistical analysis

The mean correlation coefficient, and nodal and global network measures were analysed using the MIXED procedure in IBM SPSS Statistics for Windows, version 25 (IBM Corp., N.Y., USA) according to the protocol for analysis of longitudinal data from animals with missing values using SPSS, described by Duricki et al. (2016). The covariance structure was the 'compound symmetry' structure, fixed factors were group (IPKA animals and control animals), time (baseline, 1, 3, 6, 10 and 16 weeks after SE) and group-by-time interaction. Mean ALFF in all ROIs was used as covariate. Least-significant-difference tests were used to explore significant effects and interactions, a significance level of 0.05 was used for main effects and interactions, and the Bonferroni correction was used to correct for multiple comparisons. For the analysis of nodal measures an extra correction for multiple nodal comparisons was done using the false discovery rate (FDR) at $q = 0.05$. T2-normal hippocampal

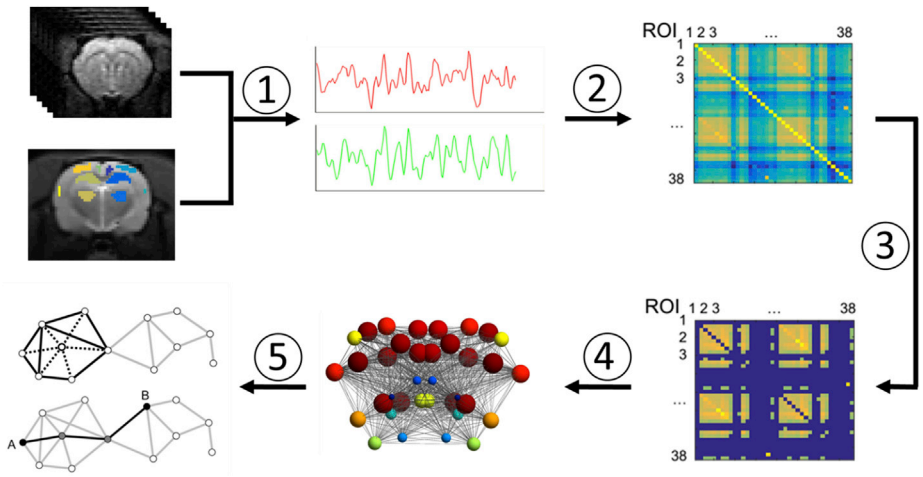

Fig. 2. Construction of a functional network and graph. 1) The mean time series of each ROI is extracted from the preprocessed rsfMRI images. 2) The Pearson correlation coefficient between each pair of ROIs is calculated and a correlation matrix is obtained. 3) A threshold is applied to remove the weakest connections. 4) The correlation matrix can be visualized as a graph in which the nodes (dots) represent the ROIs and the edges (lines) the correlation coefficients between them. 5) Several network measures can be calculated (Adapted from Rubinov and Sporns, 2010 and Wang et al., 2010).

volume was analysed in the same way, but without mean ALFF as a covariate.

The Pearson correlation coefficient was calculated between seizure frequency, i.e. the average number of seizures per day during 7 days, and mean seizure duration on the one hand, and the network measures at each time point on the other hand. In addition, the Pearson correlation was calculated between T2-normal hippocampal volume on the one hand and network measures and seizure frequency on the other hand.

2.6.7. Network-based statistic

The individual network connections were analysed with network-based statistic (NBS) using the NBS Connectome toolbox (Zalesky et al., 2010). This is a nonparametric statistical method that allows correction for multiple comparisons in a graph. The family-wise error rate is controlled when mass univariate testing is done on all connections.

The strongest network connections at baseline were identified using the One Sample Test. This test flips the sign of the data points at random for each permutation and corresponds to a one-sided One Sample *t*-test. It tests the null hypothesis that the connectivity is equal to zero. The test statistic threshold was set to 1.2 to obtain the 20% connections that differed most from zero. The ROIs that were present in the resulting subnetwork were used for further statistical analysis. The network connections that were different between IPKA and control animals were identified using the F-test with a threshold of 25.9 to obtain the 10% connections that differed the most between the groups.

3. Results

3.1. Hippocampal volume loss during epileptogenesis

The change in T2-normal hippocampal volume over time is visualized in Fig. 4. T2-normal hippocampal volume decreased significantly during epileptogenesis. Statistical analysis using the linear mixed-effects model (LMEM) showed a significant effect of group ($F_{1,24.7} = 44.9$, $p < 0.001$) and time in the IPKA group ($F_{5,122} = 26.4$, $p < 0.001$) but not in the control group ($F_{5,121} = 0.649$, $p = 0.662$). Pairwise comparison of the means showed that T2-normal hippocampal volume was significantly lower in IPKA animals compared to control animals at all time points post-SE. There was a significant decrease in T2-normal hippocampal volume in the IPKA animals between baseline and all time points post-SE.

3.2. Decrease in correlation coefficients during epileptogenesis

The difference in correlation matrices between IPKA animals and control animals is visualized in Fig. 5. All difference values were negative, indicating that the correlation coefficient between each pair of ROIs is lower in IPKA animals compared to control animals.

A similar evolution was observed in the distribution of the correlation coefficients in Fig. 6. The correlation coefficients shifted to smaller values during the development of epilepsy. This shift was already observed 1 week after status epilepticus, but the largest shift occurred 3 weeks post-SE. Later on, the distribution remained stable.

Statistical analysis of the mean correlation coefficient using LMEM showed a significant effect of group ($F_{1,27.6} = 13.68$, $p = 0.001$) and time in the IPKA group ($F_{5,127} = 8.71$, $p < 0.001$) but not in the control group ($F_{5,123} = 0.735$, $p = 0.598$). Pairwise comparison of the means showed that the mean correlation coefficient was significantly lower in IPKA animals than in controls at 3, 6, 10 and 16 weeks post-SE. In the IPKA animals, there was a significant decrease in mean correlation coefficient between baseline and 3, 6, 10 and 16 weeks post-SE and between 1 week and 3, 6 and 16 weeks post-SE. This is illustrated in Fig. 7.

3.3. Decrease in global functional segregation and integration

Significant decreases in measures of global functional segregation (i.e. clustering coefficient and local efficiency) and integration (characteristic path length and global efficiency) were observed during epileptogenesis with the largest changes occurring between 1 and 3 weeks after SE (Fig. 8). Statistical analysis of the clustering coefficient showed a significant effect of group ($F_{1,27.8} = 9.37$, $p = 0.005$) and time in the IPKA group ($F_{5,127} = 8.66$, $p < 0.001$) but not in the control group ($F_{5,123} = 0.457$, $p = 0.807$). Pairwise comparison of the means showed that clustering coefficient was significantly lower in IPKA animals compared to control animals at 3, 6, 10 and 16 weeks post-SE. There was a significant decrease in clustering coefficient in the IPKA animals between baseline and 3, 6, 10 and 16 weeks post-SE and between 1 week and 3, 6, 10 and 16 weeks post-SE. Statistical analysis of the local efficiency also showed a significant effect of group ($F_{1,26.8} = 9.96$, $p = 0.004$) and time in the IPKA group ($F_{5,126} = 8.44$, $p < 0.001$) but not in the control group ($F_{5,122} = 0.942$, $p = 0.456$). Pairwise comparison of the means showed that local efficiency was significantly lower in IPKA animals than in controls at 3, 6, 10 and 16 weeks post-SE. There was a significant decrease in local efficiency in the IPKA animals between baseline and 3 and 6 weeks post-SE and between 1 week and 3, 6, 10 and 16 weeks post-SE.

Statistical analysis of the characteristic path length showed a significant effect of group ($F_{1,26.7} = 6.70$, $p = 0.015$) and time in the IPKA group ($F_{5,126} = 10.3$, $p < 0.001$), but not in the control group ($F_{5,122} = 0.887$, $p = 0.497$). Pairwise comparison of the means showed that characteristic path length was significantly higher in IPKA animals than in control animals at 3, 6 and 10 weeks post-SE. There was a significant increase in characteristic path length in the IPKA animals

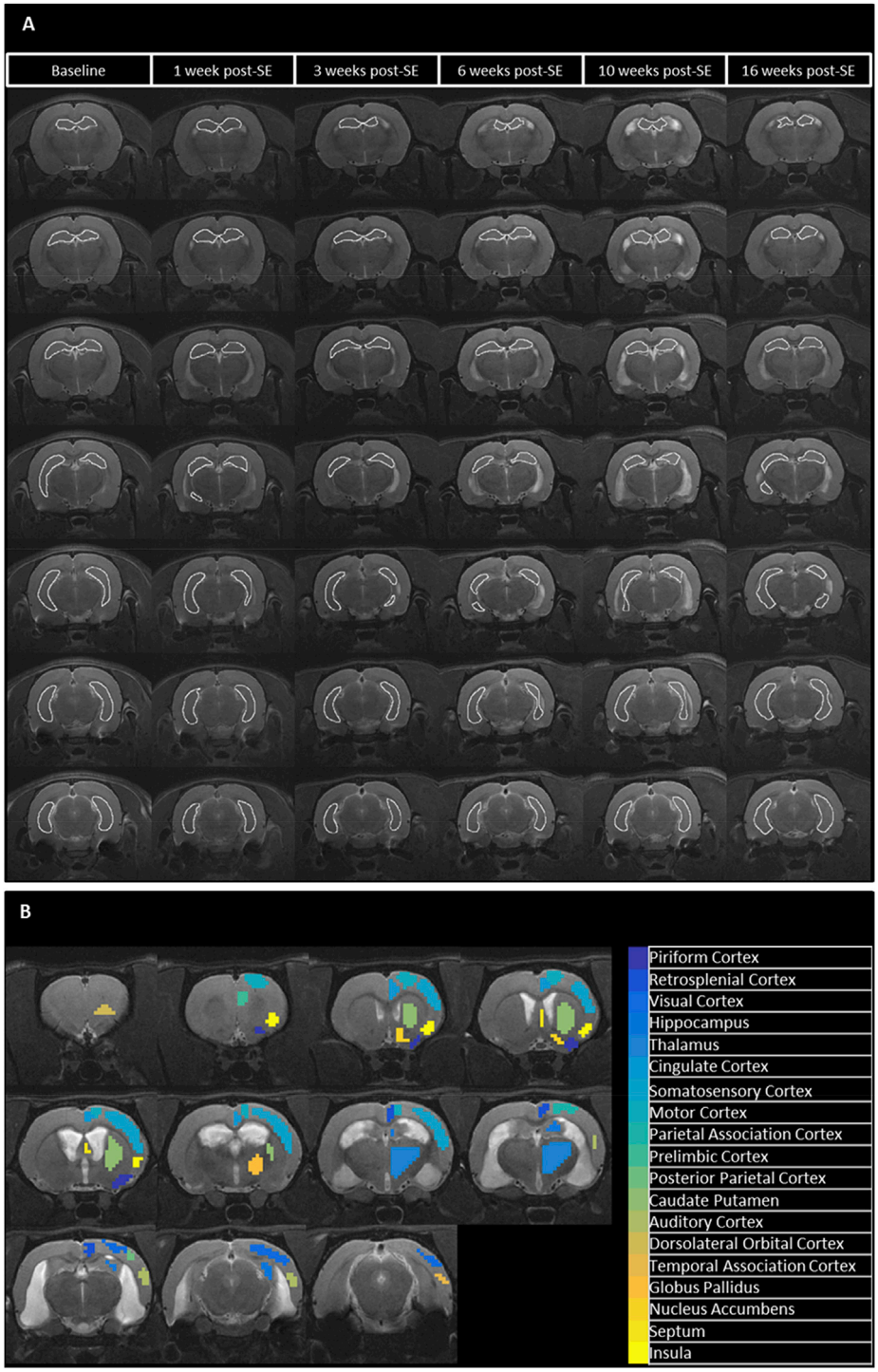

Fig. 3. A) Example of hippocampal volume loss during epileptogenesis in a representative rat. B) ROIs were adapted taking into account the most extensive structural damage (KAC4, 16 weeks post-SE). These ROIs were used to construct the functional brain network in all animals at all time points.

between baseline and 3 and 6 weeks post-SE and between 1 week and 3, 6, 10 and 16 weeks post-SE. Statistical analysis of the global efficiency showed a significant effect of group ($F_{1,26.7} = 6.89$, $p = 0.014$) and time in the IPKA group ($F_{5,126} = 8.44$, $p < 0.001$) but not in the control group ($F_{5,122} = 0.942$, $p = 0.456$). Pairwise comparison of the means showed that global efficiency was significantly lower in IPKA animals than in controls at 3, 6, 10 and 16 weeks post-SE. There was a significant decrease in global efficiency in the IPKA animals between baseline and 3 weeks post-SE and between 1 week and 3, 6 and 16 weeks post-SE.

3.4. Decrease in connectivity strength in highly connected nodes

Fig. 9 visualizes the nodal degree for each ROI at each time point. NBS was used to identify the 20% strongest connections in the network at baseline. The obtained subnetwork consisted of 20 nodes: at the left and right side of the brain; the somatosensory cortex (SSC), motor cortex (MC), caudate putamen (CPu), visual cortex (Vis), thalamus (Th), hippocampus (Hip), cingulate cortex (Cg), retrosplenial cortex (RSC), auditory cortex (Au) and parietal association cortex (PtA). These nodes were also the nodes with the highest degree at baseline and showing the

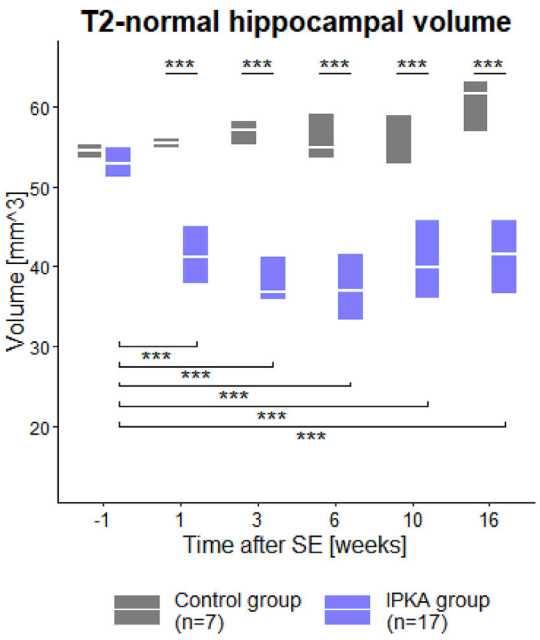

Fig. 4. T2-normal hippocampal volume over time. Data are presented as a boxplot with median and interquartile range, *p < 0.05, **p < 0.01, ***p < 0.001.

largest decreases during epileptogenesis. Because the degree of each node was similar on the right and left side of the brain, the average degree of the right and left component of each node was calculated. There was a significant effect of group and time in the IPKA group, but not in the control group (FDR-corrected $p > 0.05$) in the 10 strongest nodes. There was a significant decrease in degree during epileptogenesis and the degree was lower in the IPKA animals than in the control animals. The largest decrease happened between 1 and 3 weeks post-SE.

3.5. Decrease in connectivity in connections of the retrosplenial cortex

The most significant changes in functional connectivity take place between 1 and 3 weeks post-SE. To investigate functional connectivity changes at week 3 in more detail, NBS was used to identify which network connections differed the most between IPKA animals and controls. In Fig. 10, the 10% connections that differed the most are visualized in a circular graph ($F > 25.9$, $p < 0.001$). The majority of these connections were connected to the retrosplenial cortex (10 out of 20). Eleven out of 20 connections were within one hemisphere, the other 9 were between hemispheres. None of the connections connected the right and left component of the same brain region.

3.6. Correlation between changes in network measures and seizure frequency

Based on 7 days of consecutive EEG monitoring, the average daily seizure frequency at least 19 weeks post-SE was calculated for each animal (Fig. 11). The animal which had no seizures during the monitoring period (KAA2), did display occasional tonic-clonic seizures outside the EEG recording period (e.g. when entering the housing room). In addition, interictal epileptiform activity, such as epileptic spikes and pathological high frequency oscillations, were observed on the EEG signal (Fig. A3D). Therefore, it was considered epileptic. The relationship between the number of seizures recorded at least 19 weeks post-SE and the functional network measures was evaluated using the Pearson correlation coefficient. The Shapiro-Wilk test showed that the seizure frequency data follow a normal distribution ($W(17) = 0.953$, $p = 0.514$). Seizure frequency was positively correlated with clustering coefficient at week 1 and 16, local and global efficiency at week 1, and negatively with characteristic path length at week 1 and 16 post-SE (Figs. 12 and 13). Seizure frequency was also positively correlated with mean nodal degree measured one week post-SE, and more specifically with the degree of the hippocampus ($r = 0.591$, $p = 0.013$), thalamus ($r = 0.585$, $p = 0.014$), cingulate cortex ($r = 0.656$, $p = 0.004$), somatosensory cortex ($r = 0.617$, $p = 0.008$), caudate putamen ($r = 0.598$, $p = 0.011$), auditory cortex ($r = 0.544$, $p = 0.024$) and insula ($r = 0.653$, $p = 0.004$). No significant correlation between mean seizure duration and any of the network measures could be found.

Seizure frequency was also positively correlated with T2-normal hippocampal volume 3, 6, 10 and 16 weeks post-SE (Fig. A4). In addition, T2-normal hippocampal volume was correlated with several global network measures at all time points post-SE (Table 2).

4. Discussion

4.1. Temporal progression of network topology and link with time-dependent changes in structural lesions and seizure frequency

The aim of this study was to characterize how the topological organization of the rat brain changes after SE during the development of TLE. We found that during epileptogenesis, BOLD signal fluctuations were less correlated between brain areas, indicating decreased functional connectivity. Graph analysis revealed that segregation and integration in the functional brain network decreased during epileptogenesis. This indicates that there is a lower local interconnectivity and a lower overall communication efficiency. Nodal degree decreased significantly in the most highly connected ROIs in the baseline network, indicating a loss in connection strength. Most of these ROIs are part of the rat DMN, including cingulate cortex, retrosplenial cortex, visual cortex, auditory cortex, hippocampus, thalamus, motor cortex and somatosensory cortex (Becerra et al., 2011; Lu et al., 2012). Becerra et al. (2011) identified a spatial resting-state network that had many brain regions in common with the DMN in humans. This network consisted of the retrosplenial cortex, thalamus, hippocampus, insula, motor cortex, somatosensory cortex, orbitofrontal cortex, septum and periaqueductal gray. Later, Lu et al. (2012) demonstrated that rat brains have a DMN similar to that of humans. They identified the orbital cortex, prelimbic cortex, cingulum, auditory and temporal association cortex, posterior parietal cortex, retrosplenial cortex, hippocampus and visual cortex as its key structures. This was confirmed by Hsu et al. (2016). We also found small, non-significant changes in functional connectivity, integration and segregation in the control group, most likely due to normal aging.

Functional connectivity, segregation and integration decreased most significantly between 1 and 3 weeks post-SE. Beyond this time point, the network connectivity remained unchanged. Sharma et al. (2008) investigated the temporal progression of lesions in a kainic acid-induced rat (F-344) model of TLE. They found that neuronal degeneration can mainly be seen during the first 4 weeks after SE in the hippocampus (CA1, CA3 and dentate gyrus), amygdala, thalamus and cortex. Astrogliosis increased until 4 weeks after SE, while microgliosis peaked 1 week after SE. This gliosis remained elevated over time in these brain regions weeks after SE. Aberrant mossy fibre sprouting could be seen in the dentate gyrus 1 week after SE, reaching a maximum 2 weeks post-SE and decreasing afterwards (Sharma et al., 2008). This was confirmed by Bertoglio et al. (2017), who found neuronal loss in CA3 and dentate hilus (DH) 1 weeks post-SE and in CA3, DH and piriform cortex (Pir) 12 weeks post-SE in a kainic acid-induced rat (Sprague-Dawley) model of TLE. They also found microglial activation in CA3 and Pir 1 weeks post-SE and in Pir 12 weeks post-SE. Overall the dynamics of brain topology changes that we found, correspond nicely with the temporal profiles of neuronal degradation and gliosis. This study showed, based on structural MRI, that T2-normal hippocampal volume loss was already maximal one week after SE, indicating that the most significant change in network topology is secondary to the loss of neuronal tissue. A decreased hippocampal

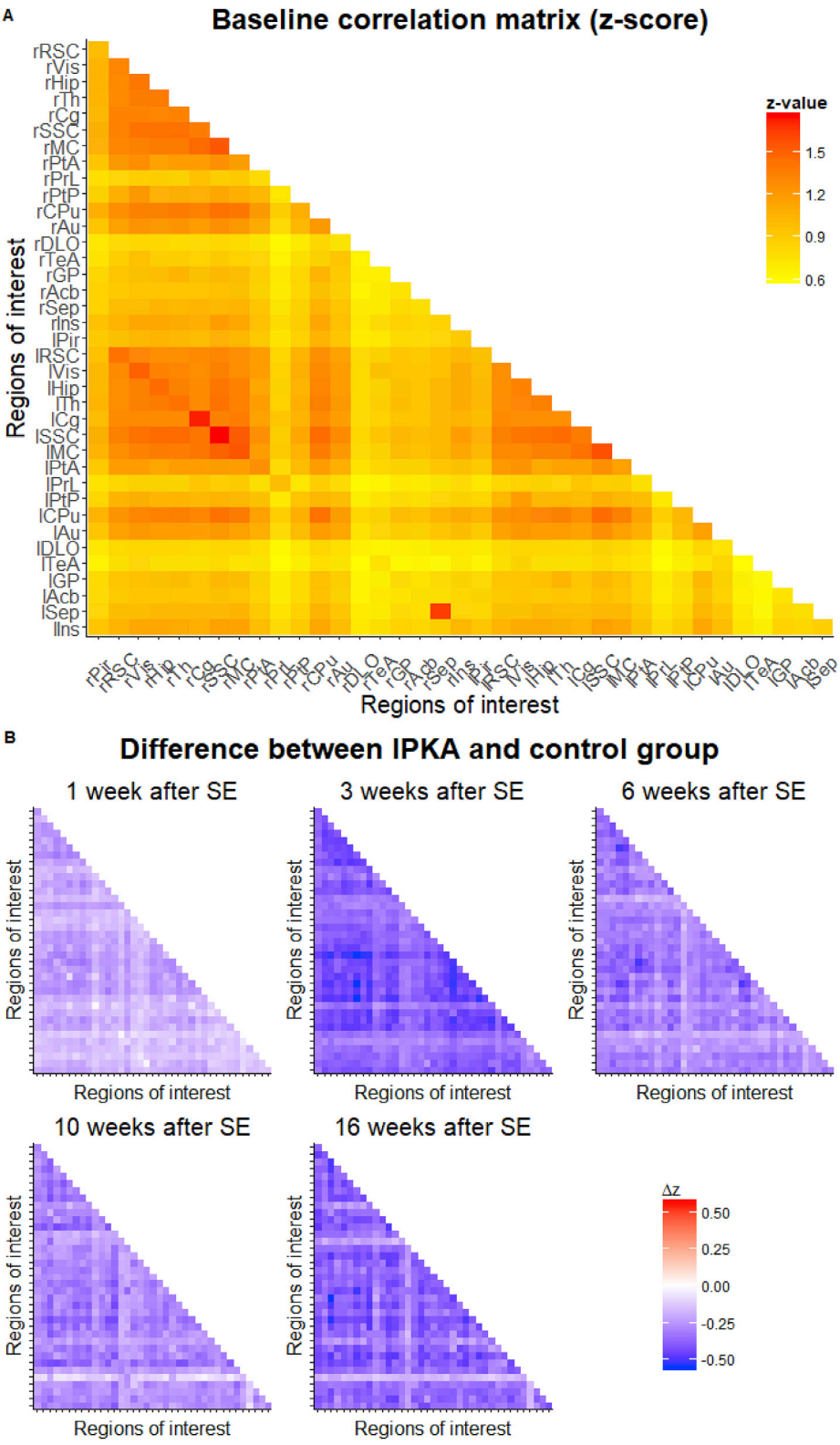

Fig. 5. Correlation matrices. A) Correlation matrix at baseline. B) Difference in correlation matrices between IPKA and control animal. All values are negative, indicating that the correlation coefficients are lower in the IPKA animals.

volume has often been reported in patients with TLE (Bernasconi et al., 2003; Briellmann et al., 2002; Lencz et al., 1992; Marsh et al., 1997).

Van Nieuwenhuyse et al. (2015) investigated how seizure frequency changes during epileptogenesis in the IPKA model and found that after a mean latency period of 7 days after SE, animals start to have spontaneous seizures at an increasing frequency until a plateau phase is reached 17 weeks after SE. While seizure frequency continues to increase 3 weeks after SE, functional connectivity, segregation and integration reached stable but decreased levels, indicating that worsening of the epileptic condition is not associated with further decrease in functional

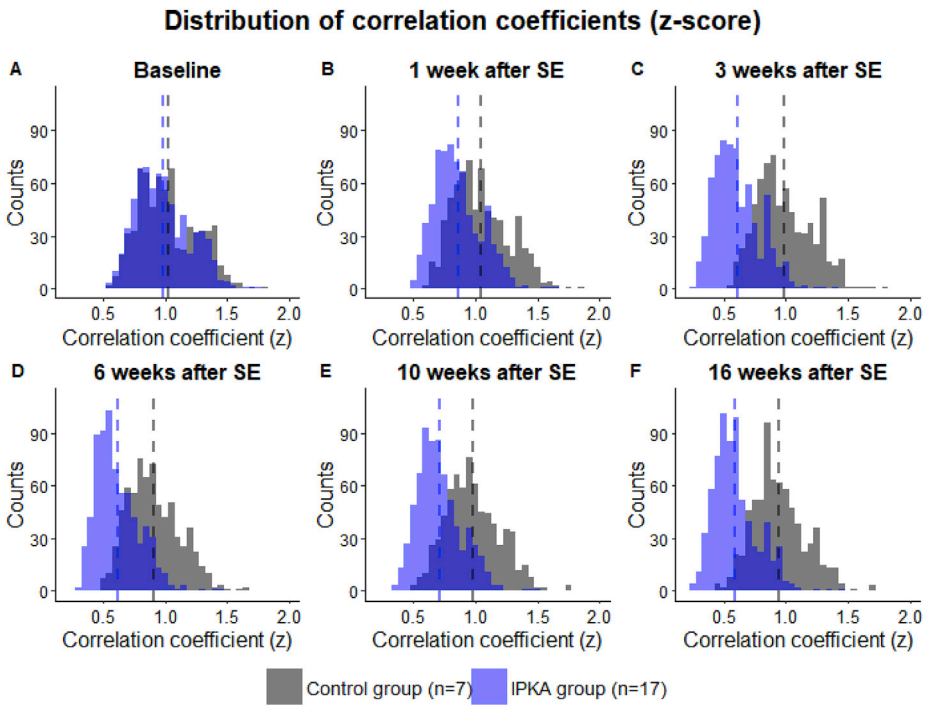

Fig. 6. Distribution of correlation coefficients (z-score). During epileptogenesis the correlation coefficients shift towards lower values in the IPKA animals.

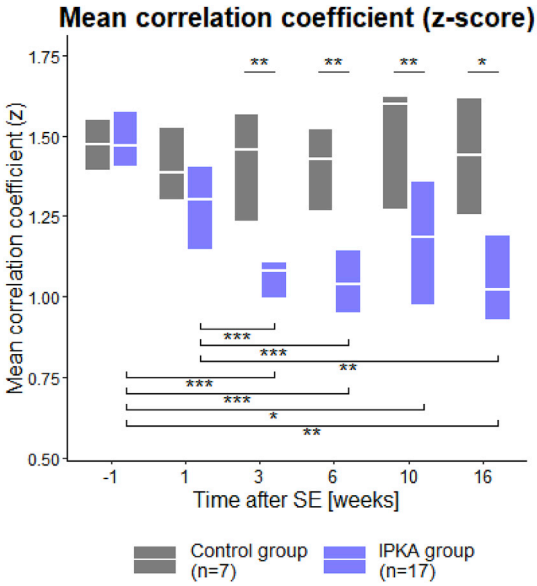

Fig. 7. Mean correlation coefficient (z-score) in function of time. The mean correlation coefficient is significantly lower in IPKA animals than in controls at 3, 6, 10 and 16 weeks post-SE. In the IPKA animals, there is a significant decrease in mean correlation coefficient between baseline and 3, 6, 10 and 16 weeks post-SE and between 1 week and 3, 6 and 16 weeks post-SE. Data are presented as a boxplot with median and interquartile range, *$p < 0.05$, **$p < 0.01$, ***$p < 0.001$.

connectivity of the brain. We cannot rule out that the animals had seizures during the image acquisition, since the used anaesthesia does not suppress seizure activity (Airaksinen et al., 2010) and EEG was not monitored during the scanning sessions. However, because seizure frequency continues to increase while network measures have reached a plateau phase, it is very unlikely that the observed changes in functional connectivity, segregation and integration are the mere result of spontaneous seizures during image acquisition.

4.2. Comparison with previous animal studies

Although there is a large variability in changes in functional connectivity and network topology during epileptogenesis between studies and animal models, most studies agree that functional connectivity is decreased in several brain regions, including hippocampus and thalamus, which corresponds with our results. Pirttimäki et al. (2016) investigated dynamic network changes in the IPKA rat model for TLE and analysed longitudinal data by comparing z-scores of correlation coefficients. They found small increases and decreases in functional connectivity in several brain regions 1 week post-SE, although the average change was not significant. Similar to our study, they found decreased functional connectivity 1 or 2 months after SE, mainly between the somatosensory cortex and thalamus and between the perirhinal and piriform cortices. An rsfMRI study performed by Mishra et al. (2014) demonstrated a lower functional connectivity between the ipsilateral and contralateral parietal cortex and between the hippocampus and parietal cortex on the injured side in the lateral fluid-percussion rat model of post-traumatic epileptogenesis 4 months post-injury, using comparison of z-scores. In the pilocarpine rat model of TLE, Jiang et al. (2018) found a decreased connectivity of the hippocampal functional network in the hippocampus, amygdala, thalamus, motor cortex and somatosensy cortex and increased connectivity in the visual cortex, mesencephalon and insula using ICA. In the IPKA model of TLE, Bertoglio et al. (2019) found a wide-spread network connectivity hyposynchrony 2 weeks post-SE, using ICA and comparison of z-scores. In addition, they found that functional connectivity was severely affected in several regions of the DMN. Interestingly, a study performed by Gill et al. (2017) in the IPKA model for TLE found a higher functional connectivity within the temporal regions and the limbic network and between the anterior and posterior DMN together with an increased network segregation and integration 4–5 weeks post-SE (Gill et al., 2017).

Several factors might contribute to the discrepancy between our study and the study by Gill et al. (2017), including different ROIs for the construction of the correlation matrix, a different animal strain (Long-Evans versus Sprague-Dawley) and the use of a different anaesthetic agent (isoflurane versus medetomidine). Several studies have shown that different types of anaesthesia have an influence on spontaneous fluctuations in the BOLD signal and on functional connectivity (Grandjean

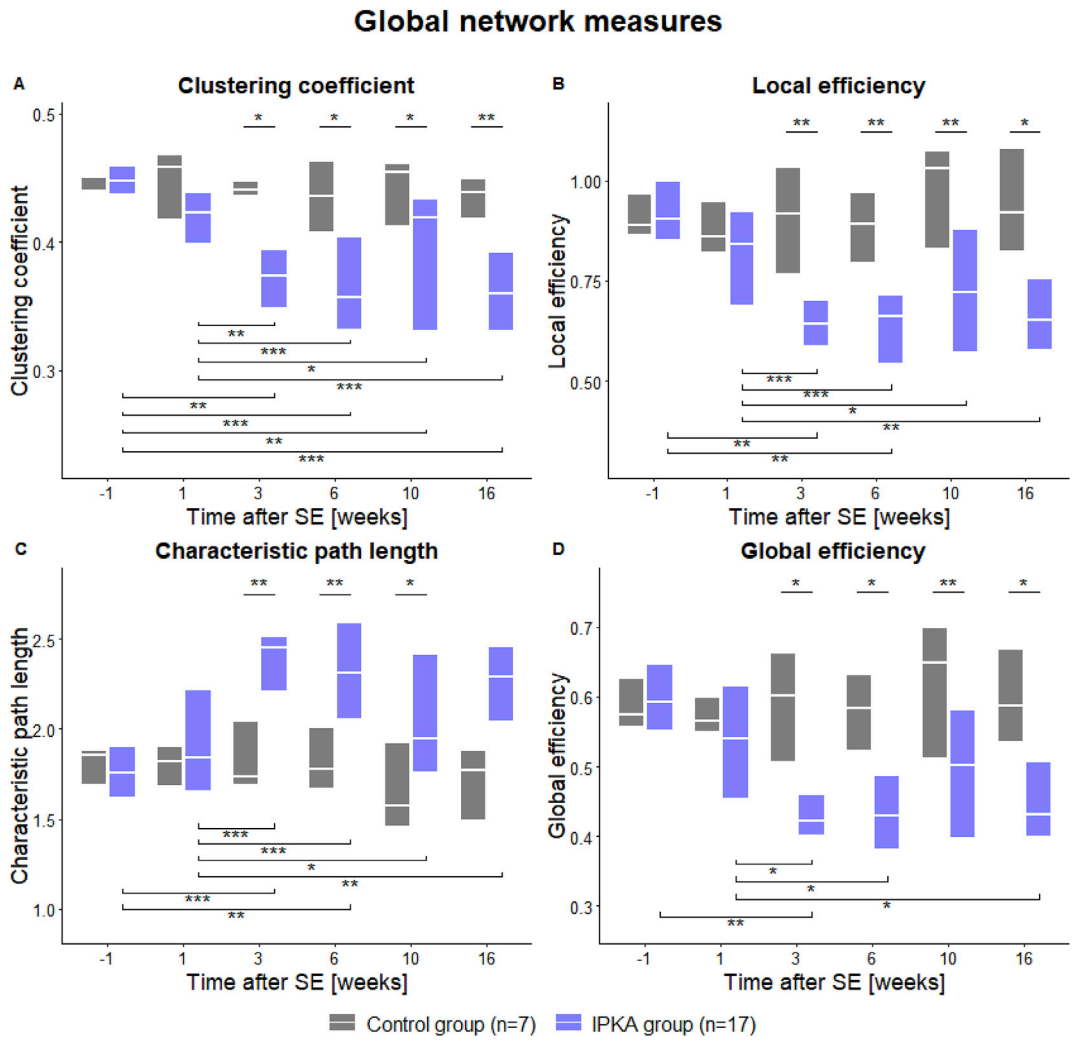

Fig. 8. Global network measures in function of time. A) Clustering coefficient and B) Local efficiency decrease during epileptogenesis, indicating a decrease in segregation in the functional network. C) Characteristic path length increases and D) Global efficiency decreases during epileptogenesis, indicating a decrease in integration. Data are presented as a boxplot with median and interquartile range, *p < 0.05, **p < 0.01, ***p < 0.001.

et al., 2014; Jonckers et al., 2014; Magnuson et al., 2014; Paasonen et al., 2018; Williams et al., 2010). Medetomidine, an α2-adrenergic agonist, has gained popularity in longitudinal fMRI studies, since it induces sedation rather than general anaesthesia and decreases global cerebral blood flow without dose-dependent vasodilation or neuronal suppression (Paasonen et al., 2016; Pan et al., 2015).

4.3. Comparison with patient studies

Our findings are generally in line with most studies investigating functional connectivity and network topology in patients with TLE. Most studies agree that segregation is decreased in patients with TLE (Liao et al., 2010; Song et al., 2015; Vlooswijk et al., 2011). Integration has been found to be increased (Liao et al., 2010; Song et al., 2015) as well as decreased (Vlooswijk et al., 2011). Liao et al. (2010) found increased functional connectivity within the temporal lobe and decreased functional connectivity in the frontal and parietal lobe and in the DMN in patients with TLE. Additionally, they found a lower degree in nodes of the DMN. Morgan et al. (2015) found that functional connectivity between the seizure propagation network and its contralateral equivalent is decreased in TLE, and that functional connectivity within the seizure propagation network decreases linearly with increasing duration of epilepsy. Pittau et al. (2012) found decreased connectivity of the hippocampus and amygdala with the DMN, ventromesial limbic prefrontal regions and contralateral mesial temporal structures including hippocampus. Song et al. (2011a) also found a decreased functional connectivity in the DMN in epilepsy patients.

4.4. Decrease in connectivity of the retrosplenial cortex

The brain region which changed most profoundly in functional connectivity in the IPKA model was the retrosplenial cortex. The retrosplenial cortex is one of the most important nodes of the rat DMN (Becerra et al., 2011; Lu et al., 2012). Three weeks post-SE, when change in network connectivity has reached stable levels, half of the connections that differ most in strength between healthy and IPKA animals, include the retrosplenial cortex. This finding is in line with a study in TLE patients that demonstrated a decrease in functional connectivity between the temporal lobe and the posterior cingulate cortex, the human equivalent of the rat retrosplenial cortex (Liao et al., 2011). It is rather surprising that the retrosplenial cortex appears to be more affected than regions of the mesial temporal lobe (hippocampus, entorhinal and piriform cortices and amygdala) which display most extensive cell loss (Lévesque and Avoli, 2013; Sharma et al., 2008). However, since the retrosplenial cortex plays a role in spatial navigation and episodic memory (Vann et al., 2009), the lower functional connectivity of this brain region could be a cause of the memory impairment seen in rats with TLE (Jiang et al., 2018).

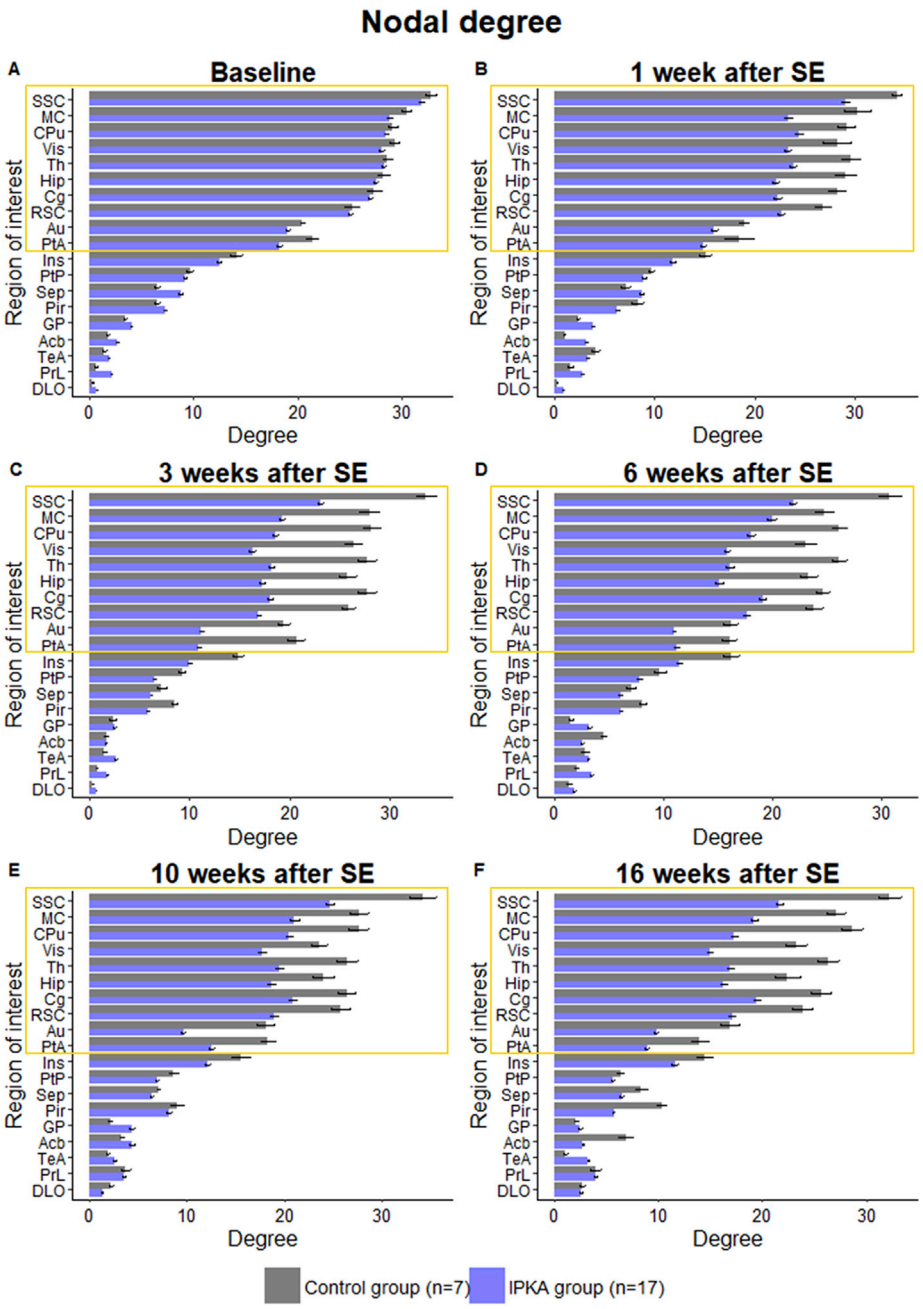

Fig. 9. Nodal degree at each time point. At baseline (A) we can see that the nodes with the highest degree (yellow rectangle) are the somatosensory cortex (SSC), motor cortex (MC), caudate putamen (CPu), visual cortex (Vis), thalamus (Th), hippocampus (Hip), cingulate cortex (Cg), retrosplenial cortex (RSC), auditory cortex (Au) and parietal association cortex (PtA). Less important nodes are the insula (Ins), posterior parietal cortex (PtP), septum (Sep), piriform cortex (Pir), globus pallidus (GP), nucleus accumbens (Acb), temporal association cortex (TeA), prelimbic cortex (PrL) and dorsolateral orbital cortex (DLO). During epileptogenesis the degree decreases in most of the nodes, especially those with a higher degree at baseline. Data are presented as a bar graph with mean and standard error.

In addition to the retrosplenial cortex, the cingulum and parietal association cortex are affected during epileptogenesis as well. These brain regions have a high structural connectivity with other cortical regions, such as hippocampus and thalamus. Together, these regions form a connection between the primary sensory cortices (Hsu et al., 2016; Lu et al., 2012). This could explain why the decrease in functional connectivity in the brain network is so extensive, rather than limited to structurally lesioned brain regions.

4.5. Correlation between changes in network measures and seizure frequency

Finally, we investigated whether the changes in network measures occurring during the development of epilepsy were associated with the occurrence of spontaneous epileptic seizures in the chronic epilepsy phase at least 19 weeks after SE. A positive correlation was found between the number of seizures on the one hand and clustering coefficient, local efficiency, global efficiency and mean degree at 1 week post-SE and clustering coefficient at 16 weeks post-SE on the other hand. A negative correlation was found with characteristic path length 1 week and 16 weeks post-SE. Seizure frequency in the chronic epilepsy phase was positively correlated with the degree of several brain regions, determined 1 week after SE. These regions included the hippocampus and thalamus, two regions heavily affected by neurodegeneration and gliosis in response to SE. So the more functionally disconnected these brain regions are upon KA-induced SE, the less likely it is for seizures to occur in the chronic phase. These associations between seizure frequency and functional connectivity measures all point out a quite unexpected finding namely that the more profound the brain network is affected by the KA-induced SE, the less likely it is that spontaneous epileptic seizures are generated. Thus it seems, the brain network needs to keep a minimal degree of organization to enable the emergence of seizures. This is in line with the potent therapeutic effects of resective/disconnective surgery as a treatment for epilepsy. Our findings correspond with those of Bertoglio

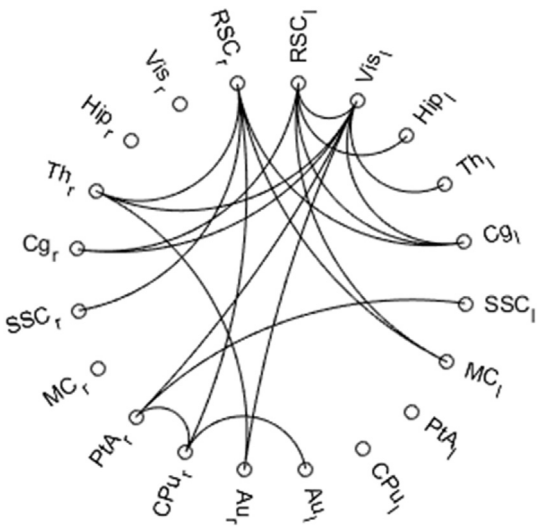

Fig. 10. Circular visualisation of network with the 10% connections that differ the most between IPKA and control animals 3 weeks post-SE. Half of the connections are connections of the retrosplenial cortex.

et al. (2019), who also found that functional connectivity is correlated with seizure frequency. In addition, we found that animals with the largest T2-normal hippocampal volume loss, displayed the lowest number of seizures. This could indicate that a sufficient amount of hippocampal tissue needs to be preserved as substrate for seizure generation.

The correlation between network measures and seizure frequency 1 week after SE is very interesting, since we never recorded spontaneous epileptic seizures at that time point in the IPKA model for TLE. This indicates that network reorganisation upon an IPI might have a predictive value and could potentially be used a biomarker for the development and progression of epilepsy.

4.6. Study limitations

To calculate mean seizure frequency and duration, seizures were visually annotated by experienced investigators. Our study could have benefitted from automated seizure detection. In preclinical epilepsy research, automatic seizure detection is rarely used and visual annotation remains the standard procedure. Seizures are easy to recognize by a trained researcher, but hard to describe in terms of parameters, because they are complex and slightly different in every animal. However, with recent advances in machine learning, automatic detection is starting to emerge.

EEG was recorded for 7 consecutive days and seizures were detected in all IPKA animals but one (KAA2). Since this animal did display

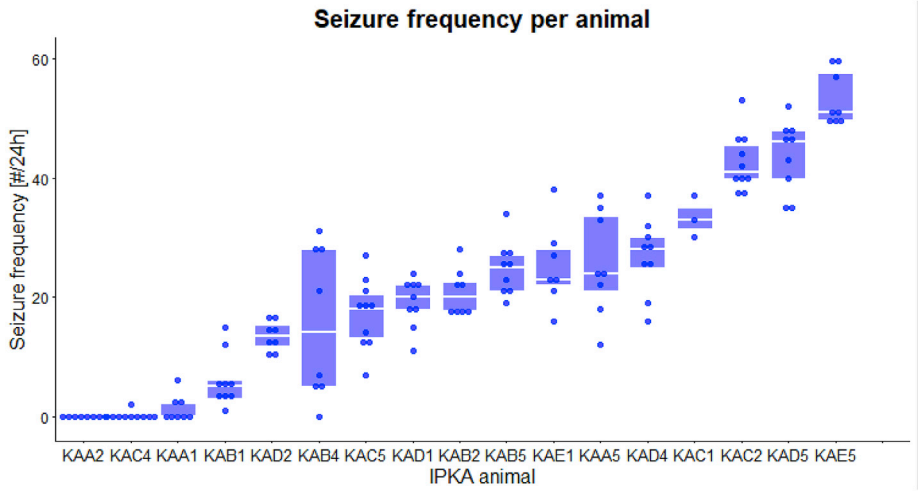

Fig. 11. Seizure frequency (# per 24 h) per animal. Data are presented as a boxplot with median, interquartile range and individual data points.

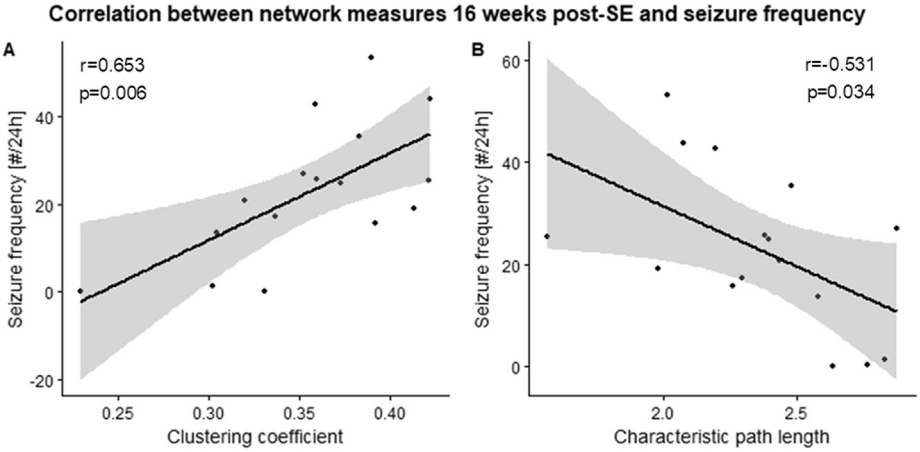

Fig. 12. Correlation between network measures 16 weeks post-SE and seizure frequency (number per 24 h).

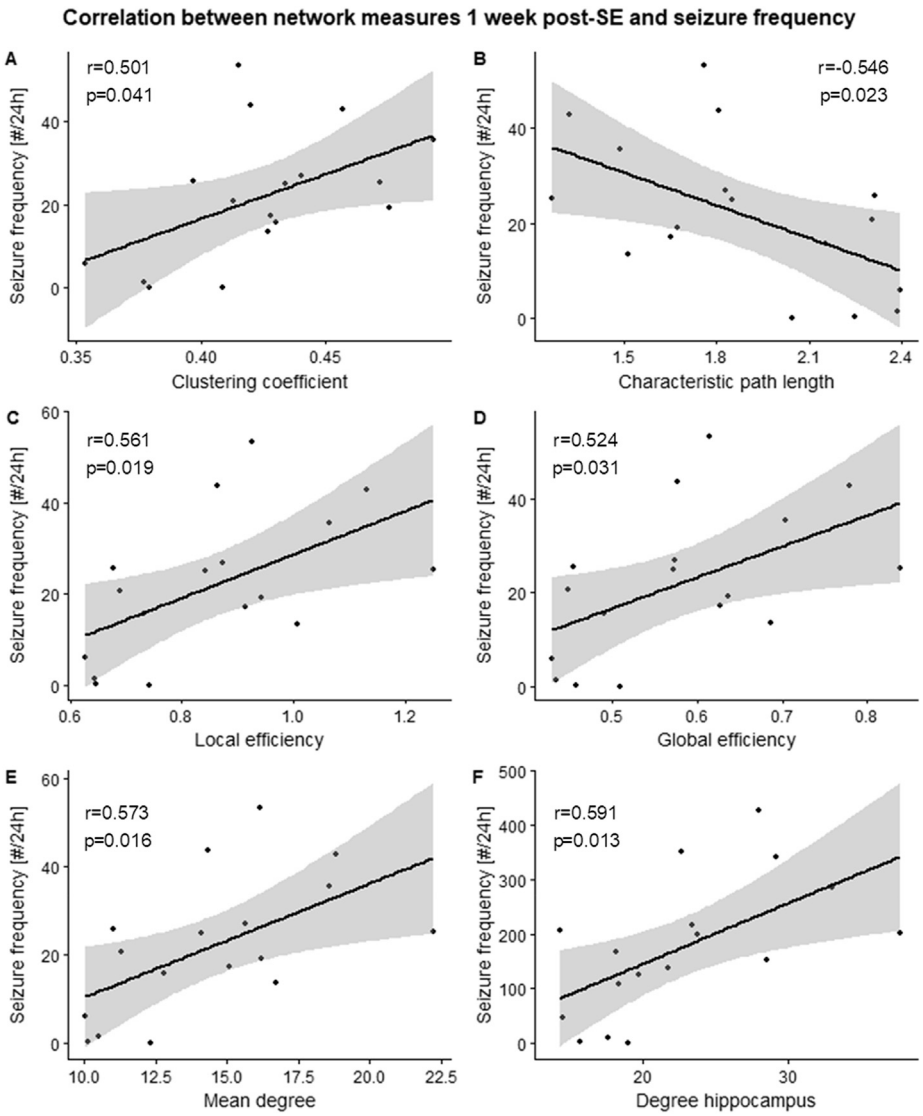

Fig. 13. Correlation between network measures 1 week post-SE and seizure frequency (number per 24 h).

Table 2
Correlation between T2-normal hippocampal volume and seizure frequency and global network measures (*p < 0.05, **p < 0.01, ***p < 0.001).

			Seizure frequency [#/24 h]	Mean degree	Clustering coefficient	Characteristic path length	Local efficiency	Global efficiency
						1 week post-SE		
T2-normal hippocampal volume	1 week post-SE	r	0.281	0.501*	0.519*	−0.543*	0.542*	0.545*
		p	0.275	0.034	0.027	0.020	0.020	0.019
						3 weeks post-SE		
	3 weeks post-SE	r	0.751**	0.451	0.389	−0.671**	0.502*	0.537*
		p	0.001	0.070	0.123	0.003	0.040	0.026
						6 weeks post-SE		
	6 weeks post-SE	r	0.636**	0.579*	0.404	−0.598*	0.578*	0.566*
		p	0.008	0.015	0.108	0.011	0.015	0.018
						10 weeks post-SE		
	10 weeks post-SE	r	0.614*	0.775***	0.777***	−0.823***	0.777***	0.786***
		p	0.011	<0.001	<0.001	<0.001	<0.001	<0.001
						16 weeks post-SE		
	16 weeks post-SE	r	0.709**	0.636**	0.760***	−0.684**	0.674**	0.631**
		p	0.002	0.006	<0.001	0.002	0.003	0.007

occasional tonic-clonic seizures outside the EEG recording period, a longer recording period might be recommended to obtain a more accurate estimate of the seizure frequency.

Another limitation of our study is that we did not do post-mortem histological analysis. Therefore, we could not confirm the extent of hippocampal volume loss calculated based on the T2 images, nor could we verify the exact location of the electrodes, which would have been particularly interesting in the animals with extensive damage. In

addition, we could not investigate whether the changes in network topology during epileptogenesis were related to specific histopathological changes, such as neuronal loss or gliosis.

Finally, we calculated the volume of the hippocampus by delineating hippocampal tissue that looked normal on the T2-weighted MR images (Wolf et al., 2002). To avoid including ventricles in the volume of the hippocampus, all hyperintensities were excluded, since it was difficult to differentiate between enlarged ventricles and other reasons for hyperintensities, such as gliosis or inflammation. This means that we measured T2-normal hippocampal volume, and not the actual volume of the hippocampus. The T2-normal hippocampal volume is most likely an underestimation of the actual volume.

5. Conclusion

We investigated changes in functional brain networks during epileptogenesis in the IPKA rat model of TLE using longitudinal resting state fMRI and graph theory. First, we found that functional brain network connections become weaker during the development of epilepsy. On a global level, we found that segregation and integration in the functional brain network decrease during epileptogenesis. As hypothesized, the functional brain network was extensively disrupted during the development of epilepsy. The largest changes in functional connectivity, segregation and integration occurred between 1 and 3 weeks post-SE, which is when the animals start to have spontaneous seizures. A loss in connection strength could be seen in the most highly connected ROIs in the network, many of which are part of the rat DMN. Secondly, we found that 3 weeks post-SE, the connectivity of the retrosplenial cortex, one of the most important nodes in the rat DMN, was highly affected. Lastly, as we hypothesized, the changes in functional connectivity, segregation and integration were correlated with seizure frequency. A more profound topological reorganisation of the brain network corresponds with a lower frequency of spontaneous epileptic seizures. The findings of this study provide more insight into how the topological organization of the functional brain network changes during the development of epilepsy, which could lead to a better understanding of the underlying mechanisms of epilepsy and help the rational development of epilepsy therapies. To further elaborate on the link between changes in brain network topology and epileptogenesis, a follow-up study is planned using MR-compatible electrodes to enable longitudinal EEG-fMRI studies in various models for acquired epilepsy, including the IPKA animal model.

Declaration of interest

This research was financially supported by a PhD grant from the Special Research Fund (BOF; project number BOF24J2016000601) of Ghent University. Emma Christiaen, Marie-Gabrielle Goossens and Erine Craey are SB PhD fellows at Research Foundation – Flanders (project numbers 1S90218N, 1S30017N and 1S65519N). The authors have no competing interests to declare.

Appendix A. Supplementary data

Supplementary data to this article can be found online at https://doi.org/10.1016/j.neuroimage.2019.116144.

References

Airaksinen, A.M., Niskanen, J.-P., Chamberlain, R., Huttunen, J.K., Nissinen, J., Garwood, M., Pitkänen, A., Gröhn, O., 2010. Simultaneous fMRI and local field potential measurements during epileptic seizures in medetomidine-sedated rats using raser pulse sequence. Magn. Reson. Med. 64, 1191–1199. https://doi.org/10.1002/mrm.22508.

Becerra, L., Pendse, G., Chang, P.-C., Bishop, J., Borsook, D., 2011. Robust reproducible resting state networks in the awake rodent brain. PLoS One 6, e25701. https://doi.org/10.1371/journal.pone.0025701.

Bernasconi, N., Bernasconi, A., Caramanos, Z., Antel, S.B., Andermann, F., Arnold, D.L., 2003. Mesial temporal damage in temporal lobe epilepsy: a volumetric MRI study of the hippocampus, amygdala and parahippocampal region. Brain 126, 462–469. https://doi.org/10.1093/brain/awg034.

Bertoglio, D., Amhaoul, H., Van Eetveldt, A., Houbrechts, R., Van De Vijver, S., Ali, I., Dedeurwaerdere, S., 2017. Kainic acid-induced post-status epilepticus models of temporal lobe epilepsy with diverging seizure phenotype and neuropathology. Front. Neurol. 8, 588. https://doi.org/10.3389/fneur.2017.00588.

Bertoglio, D., Jonckers, E., Ali, I., Verhoye, M., Van der Linden, A., Dedeurwaerdere, S., 2019. In vivo measurement of brain network connectivity reflects progression and intrinsic disease severity in a model of temporal lobe epilepsy. Neurobiol. Dis. 127, 45–52. https://doi.org/10.1016/J.NBD.2019.02.012.

Briellmann, R.S., Berkovic, S.F., Syngeniotis, A., King, M.A., Jackson, G.D., 2002. Seizure-associated hippocampal volume loss: a longitudinal magnetic resonance study of temporal lobe epilepsy. Ann. Neurol. 51, 641–644. https://doi.org/10.1002/ana.10171.

Di, X., Kim, E.H., Huang, C.-C., Tsai, S.-J., Lin, C.-P., Biswal, B.B., 2013. The influence of the amplitude of low-frequency fluctuations on resting-state functional connectivity. Front. Hum. Neurosci. 7, 118. https://doi.org/10.3389/fnhum.2013.00118.

Duricki, D.A., Soleman, S., Moon, L.D.F., 2016. Analysis of longitudinal data from animals with missing values using SPSS. Nat. Protoc. 11, 1112–1129. https://doi.org/10.1038/nprot.2016.048.

Engel Jr., J., 2014. Approaches to refractory epilepsy. Ann. Indian Acad. Neurol. 17, S12–S17. https://doi.org/10.4103/0972-2327.128644.

Fisher, R.S., Boas, W. van E., Blume, W., Elger, C., Genton, P., Lee, P., Engel, J., 2005. Epileptic seizures and epilepsy: definitions proposed by the international league against epilepsy (ILAE) and the international bureau for epilepsy (IBE). Epilepsia 46, 470–472. https://doi.org/10.1111/j.0013-9580.2005.66104.x.

Fornito, A., Zalesky, A., Bullmore, E.T., 2010. Network scaling effects in graph analytic studies of human resting-state fMRI data. Front. Syst. Neurosci. 4, 22. https://doi.org/10.3389/fnsys.2010.00022.

Gill, R.S., Mirsattari, S.M., Leung, L.S., 2017. Resting state functional network disruptions in a kainic acid model of temporal lobe epilepsy. Neuroimage Clin. 13, 70–81. https://doi.org/10.1016/j.nicl.2016.11.002.

Goldberg, E.M., Coulter, D.A., 2013. Mechanisms of epileptogenesis: a convergence on neural circuit dysfunction. Nat. Rev. Neurosci. 14, 337–349. https://doi.org/10.1038/nrn3482.

Grandjean, J., Schroeter, A., Batata, I., Rudin, M., 2014. Optimization of anesthesia protocol for resting-state fMRI in mice based on differential effects of anesthetics on functional connectivity patterns. Neuroimage 102, 838–847. https://doi.org/10.1016/J.NEUROIMAGE.2014.08.043.

Hellier, J.L., Patrylo, P.R., Buckmaster, P.S., Dudek, F.E., 1998. Recurrent spontaneous motor seizures after repeated low-dose systemic treatment with kainate: assessment of a rat model of temporal lobe epilepsy. Epilepsy Res. 31, 73–84.

Hsu, L.-M., Liang, X., Gu, H., Brynildsen, J.K., Stark, J.A., Ash, J.A., Lin, C.-P., Lu, H., Rapp, P.R., Stein, E.A., Yang, Y., 2016. Constituents and functional implications of the rat default mode network. Proc. Natl. Acad. Sci. U. S. A 113, E4541–E4547. https://doi.org/10.1073/pnas.1601485113.

Jiang, Y., Han, C.-L., Liu, H.-G., Wang, X., Zhang, X., Meng, F.-G., Zhang, J.-G., 2018. Abnormal hippocampal functional network and related memory impairment in pilocarpine-treated rats. Epilepsia 59, 1785–1795. https://doi.org/10.1111/epi.14523.

Jonckers, E., Delgado y Palacios, R., Shah, D., Guglielmetti, C., Verhoye, M., Van der Linden, A., 2014. Different anesthesia regimes modulate the functional connectivity outcome in mice. Magn. Reson. Med. 72, 1103–1112. https://doi.org/10.1002/mrm.24990.

Jutila, L., Ylinen, A., Partanen, K., Alafuzoff, I., Mervaala, E., Partanen, J., Vapalahti, M., Vainio, P., Pitkänen, A., 2001. MR volumetry of the entorhinal, perirhinal, and temporopolar cortices in drug-refractory temporal lobe epilepsy. Am. Soc. Neuroradiol. 22, 1490–1501.

Kwan, P., Brodie, M.J., 2000. Early identification of refractory epilepsy. N. Engl. J. Med. 342, 314–319. https://doi.org/10.1056/NEJM200002033420503.

Lencz, T., McCarthy, G., Bronen, R.A., Scott, T.M., Inserni, J.A., Sass, K.J., Novelly, R.A., Kim, J.H., Spencer, D.D., 1992. Quantitative magnetic resonance imaging in temporal lobe epilepsy: relationship to neuropathology and neuropsychological function. Ann. Neurol. 31, 629–637. https://doi.org/10.1002/ana.410310610.

Lévesque, M., Avoli, M., 2013. The kainic acid model of temporal lobe epilepsy. Neurosci. Biobehav. Rev. 37, 2887–2899. https://doi.org/10.1016/J.NEUBIOREV.2013.10.011.

Liao, W., Zhang, Z., Pan, Z., Mantini, D., Ding, J., Duan, X., Luo, C., Lu, G., Chen, H., 2010. Altered functional connectivity and small-world in mesial temporal lobe epilepsy. PLoS One 5, e8525. https://doi.org/10.1371/journal.pone.0008525.

Liao, W., Zhang, Z., Pan, Z., Mantini, D., Ding, J., Duan, X., Luo, C., Wang, Z., Tan, Q., Lu, G., Chen, H., 2011. Default mode network abnormalities in mesial temporal lobe epilepsy: a study combining fMRI and DTI. Hum. Brain Mapp. 32, 883–895. https://doi.org/10.1002/hbm.21076.

Lu, H., Zou, Q., Gu, H., Raichle, M.E., Stein, E.A., Yang, Y., 2012. Rat brains also have a default mode network. Proc. Natl. Acad. Sci. U. S. A 109, 3979–3984. https://doi.org/10.1073/pnas.1200506109.

Magnuson, M.E., Thompson, G.J., Pan, W.-J., Keilholz, S.D., 2014. Time-dependent effects of isoflurane and dexmedetomidine on functional connectivity, spectral characteristics, and spatial distribution of spontaneous BOLD fluctuations. NMR Biomed. 27, 291–303. https://doi.org/10.1002/nbm.3062.

Marsh, L., Morrell, M.J., Shear, P.K., Sullivan, E.V., Freeman, H., Marie, A., Lim, K.O., Pfefferbaum, A., 1997. Cortical and hippocampal volume deficits in temporal lobe epilepsy. Epilepsia 38, 576–587. https://doi.org/10.1111/j.1528-1157.1997.tb01143.x.

Matthews, P.M., Jezzard, P., 2004. Functional magnetic resonance imaging. J. Neurol. Neurosurg. Psychiatry 75, 6–12.

Mishra, A.M., Bai, X., Sanganahalli, B.G., Waxman, S.G., Shatillo, O., Grohn, O., Hyder, F., Pitkänen, A., Blumenfeld, H., 2014. Decreased resting functional connectivity after traumatic brain injury in the rat. PLoS One 9, e95280. https://doi.org/10.1371/journal.pone.0095280.

Morgan, V.L., Abou-Khalil, B., Rogers, B.P., 2015. Evolution of functional connectivity of brain networks and their dynamic interaction in temporal lobe epilepsy. Brain Connect. 5, 35–44. https://doi.org/10.1089/brain.2014.0251.

Nairismagi, J., Pitkanen, A., Kettunen, M.I., Kauppinen, R.A., Kubova, H., 2006. Status epilepticus in 12-day-old rats leads to temporal lobe neurodegeneration and volume reduction: a histologic and MRI study. Epilepsia 47, 479–488. https://doi.org/10.1111/j.1528-1167.2006.00455.x.

Niessen, H.G., Angenstein, F., Vielhaber, S., Frisch, C., Kudin, A., Elger, C.E., Heinze, H.-J., Scheich, H., Kunz, W.S., 2005. Volumetric magnetic resonance imaging of functionally relevant structural alterations in chronic epilepsy after pilocarpine-induced status epilepticus in rats. Epilepsia 46, 1021–1026. https://doi.org/10.1111/j.1528-1167.2005.60704.x.

Otte, W.M., Dijkhuizen, R.M., van Meer, M.P.A., van der Hel, W.S., Verlinde, S.A.M.W., van Nieuwenhuizen, O., Viergever, M.A., Stam, C.J., Braun, K.P.J., 2012. Characterization of functional and structural integrity in experimental focal epilepsy: reduced network efficiency coincides with white matter changes. PLoS One 7, e39078. https://doi.org/10.1371/journal.pone.0039078.

Paasonen, J., Salo, R.A., Shatillo, A., Forsberg, M.M., Närväinen, J., Huttunen, J.K., Gröhn, O., 2016. Comparison of seven different anesthesia protocols for nicotine pharmacologic magnetic resonance imaging in rat. Eur. Neuropsychopharmacol. 26, 518–531. https://doi.org/10.1016/J.EURONEURO.2015.12.034.

Paasonen, J., Stenroos, P., Salo, R.A., Kiviniemi, V., Gröhn, O., 2018. Functional connectivity under six anesthesia protocols and the awake condition in rat brain. Neuroimage 172, 9–20. https://doi.org/10.1016/J.NEUROIMAGE.2018.01.014.

Pan, W.-J., Billings, J.C.W., Grooms, J.K., Shakil, S., Keilholz, S.D., 2015. Considerations for resting state functional MRI and functional connectivity studies in rodents. Front. Neurosci. 9, 269. https://doi.org/10.3389/fnins.2015.00269.

Paxinos, G., Watson, C., 2013. The Rat Brain in Stereotaxic Coordinates : Hard, Cover Edition. Elsevier Science.

Pirttimäki, T., Salo, R.A., Shatillo, A., Kettunen, M.I., Paasonen, J., Sierra, A., Jokivarsi, K., Leinonen, V., Andrade, P., Quittek, S., Pitkänen, A., Gröhn, O., 2016. Implantable RF-coil with multiple electrodes for long-term EEG-fMRI monitoring in rodents. J. Neurosci. Methods 274, 154–163. https://doi.org/10.1016/j.jneumeth.2016.10.014.

Pittau, F., Grova, C., Moeller, F., Dubeau, F., Gotman, J., 2012. Patterns of altered functional connectivity in mesial temporal lobe epilepsy. Epilepsia 53, 1013–1023. https://doi.org/10.1111/j.1528-1167.2012.03464.x.

Polli, R.S., Malheiros, J.M., Dos Santos, R., Hamani, C., Longo, B.M., Tannús, A., Mello, L.E., Covolan, L., 2014. Changes in hippocampal volume are correlated with cell loss but not with seizure frequency in two chronic models of temporal lobe epilepsy. Front. Neurol. 5, 111. https://doi.org/10.3389/fneur.2014.00111.

Rubinov, M., Sporns, O., 2010. Complex network measures of brain connectivity : uses and interpretations. Neuroimage 52, 1059–1069. https://doi.org/10.1016/j.neuroimage.2009.10.003.

Rueden, C.T., Schindelin, J., Hiner, M.C., DeZonia, B.E., Walter, A.E., Arena, E.T., Eliceiri, K.W., 2017. ImageJ2: ImageJ for the next generation of scientific image data. BMC Bioinf. 18, 529. https://doi.org/10.1186/s12859-017-1934-z.

Schindelin, J., Arganda-Carreras, I., Frise, E., Kaynig, V., Longair, M., Pietzsch, T., Preibisch, S., Rueden, C., Saalfeld, S., Schmid, B., Tinevez, J.-Y., White, D.J., Hartenstein, V., Eliceiri, K., Tomancak, P., Cardona, A., 2012. Fiji: an open-source platform for biological-image analysis. Nat. Methods 9, 676–682. https://doi.org/10.1038/nmeth.2019.

Sharma, A.K., Jordan, W.H., Reams, R.Y., Hall, D.G., Snyder, P.W., 2008. Temporal profile of clinical signs and histopathologic changes in an F-344 rat model of kainic acid–induced mesial temporal lobe epilepsy. Toxicol. Pathol. 36, 932–943. https://doi.org/10.1177/0192623308326093.

Smitha, K.A., Akhil Raja, K., Arun, K.M., Rajesh, P.G., Thomas, B., Kapilamoorthy, T.R., Kesavadas, C., 2017. Resting state fMRI: a review on methods in resting state connectivity analysis and resting state networks. Neuroradiol. J. 30, 305–317. https://doi.org/10.1177/1971400917697342.

Song, J., Nair, V.A., Gaggl, W., Prabhakaran, V., 2015. Disrupted brain functional organization in epilepsy revealed by graph theory analysis. Brain Connect. 5, 276–283. https://doi.org/10.1089/brain.2014.0308.

Song, M., Du, H., Wu, N., Hou, B., Wu, G., Wang, J., Feng, H., Jiang, T., 2011a. Impaired resting-state functional integrations within default mode network of generalized tonic-clonic seizures epilepsy. PLoS One 6, e17294. https://doi.org/10.1371/journal.pone.0017294.

Song, X.-W., Dong, Z.-Y., Long, X.-Y., Li, S.-F., Zuo, X.-N., Zhu, C.-Z., He, Y., Yan, C.-G., Zang, Y.-F., 2011b. REST: a Toolkit for resting-state functional magnetic resonance imaging data processing. PLoS One 6, e25031. https://doi.org/10.1371/journal.pone.0025031.

Van Nieuwenhuyse, B., Raedt, R., Sprengers, M., Dauwe, I., Gadeyne, S., Carrette, E., Delbeke, J., Wadman, W.J., Boon, P., Vonck, K., 2015. The systemic kainic acid rat model of temporal lobe epilepsy: long-term EEG monitoring. Brain Res. 1627, 1–11. https://doi.org/10.1016/j.brainres.2015.08.016.

Vann, S.D., Aggleton, J.P., Maguire, E.A., 2009. What does the retrosplenial cortex do? Nat. Rev. Neurosci. 10, 792–802. https://doi.org/10.1038/nrn2733.

Vlooswijk, M.C.G., Vaessen, M.J., Jansen, J.F.A., de Krom, M.C.F.T.M., Majoie, H.J.M., Hofman, P.A.M., Aldenkamp, A.P., Backes, W.H., 2011. Loss of network efficiency associated with cognitive decline in chronic epilepsy. Neurology 77, 938–944. https://doi.org/10.1212/WNL.0b013e31822cfc2f.

Wang, J., Wang, X., Xia, M., Liao, X., Evans, A., He, Y., 2015. GRETNA: a graph theoretical network analysis toolbox for imaging connectomics. Front. Hum. Neurosci. 9, 386. https://doi.org/10.3389/fnhum.2015.00386.

Wang, J., Zuo, X., He, Y., 2010. Graph-based network analysis of resting-state functional MRI. Front. Syst. Neurosci. 4, 16. https://doi.org/10.3389/fnsys.2010.00016.

Weber, R., Ramos-Cabrer, P., Wiedermann, D., van Camp, N., Hoehn, M., 2006. A fully noninvasive and robust experimental protocol for longitudinal fMRI studies in the rat. Neuroimage 29, 1303–1310. https://doi.org/10.1016/J.NEUROIMAGE.2005.08.028.

Williams, K.A., Magnuson, M., Majeed, W., LaConte, S.M., Peltier, S.J., Hu, X., Keilholz, S.D., 2010. Comparison of alpha-chloralose, medetomidine and isoflurane anesthesia for functional connectivity mapping in the rat. Magn. Reson. Imaging 28, 995–1003. https://doi.org/10.1016/j.mri.2010.03.007.

Wolf, O., Dyakin, V., Patel, A., Vadasz, C., de Leon, M., McEwen, B., Bulloch, K., 2002. Volumetric structural magnetic resonance imaging (MRI) of the rat hippocampus following kainic acid (KA) treatment. Brain Res. 934, 87–96. https://doi.org/10.1016/S0006-8993(02)02363-6.

Zalesky, A., Fornito, A., Bullmore, E.T., 2010. Network-based statistic: identifying differences in brain networks. Neuroimage 53, 1197–1207. https://doi.org/10.1016/J.NEUROIMAGE.2010.06.041.